

# Photorealistic Models for Pupil Light Reflex and Iridal Pattern Deformation

VITOR F. PAMPLONA and MANUEL M. OLIVEIRA

Instituto de Informática - UFRGS, Brazil

and

GLADIMIR V. G. BARANOSKI

Natural Phenomena Simulation Group - University of Waterloo, Canada



---

We introduce a physiologically-based model for pupil light reflex (PLR) and an image-based model for iridal pattern deformation. Our PLR model expresses the pupil diameter as a function of the environment lighting, and is described by a delay-differential equation, naturally adapting the pupil diameter even to abrupt changes in light conditions. Since the parameters of our PLR model were derived from measured data, it correctly simulates the actual behavior of the human pupil. Another contribution of our work is a model for realist deformation of the iris pattern as a function of pupil dilation and constriction. Our models produce high-fidelity appearance effects and can be used to produce real-time predictive animations of the pupil and iris under variable lighting conditions. We assess the predictability and quality of our simulations through comparisons of modeled results against measured data derived from experiments also described in this work. Combined, our models can bring facial animation to new photorealistic standards.

Categories and Subject Descriptors: I.3.7 [**Computer Graphics**]: Three-Dimensional Graphics and Realism—*Animation*; I.3.5 [**Computer Graphics**]: Computational Geometry and Object Modeling—*Physically based modeling*

General Terms: Experimentation, Human Factors

Additional Key Words and Phrases: face animation, image-based modelling, iris animation, photorealism, physiologically-based modelling

---

## 1. INTRODUCTION

Arguably, the most important feature in facial animation are the eyes, which are essential not only in directing the gaze of the audience [Lee et al. 2002], but also in conveying the appropriate degree of expression through pupil dilation and constriction movements [Watt and Watt 1992]. Hence, for animations depicting close-up views of the face, natural-looking eyes and pupil movements are highly desirable.

Walt Disney once said to his animation team that the audience watches the eyes and this is where the time and money must be spent if the character is to act convincingly [Watt and Watt 1992].

Differently from most of the body, the human eye is subject to some involuntary movements of the pupil, which are determined by ambient illumination, drug action, and emotional conditions, among others [Reeves

---

Authors' emails: vitor@vitorpamplona.com, oliveira@inf.ufrgs.br and gvgbaran@curumin.math.uwaterloo.ca

Permission to make digital/hard copy of all or part of this material without fee for personal or classroom use provided that the copies are not made or distributed for profit or commercial advantage, the ACM copyright/server notice, the title of the publication, and its date appear, and notice is given that copying is by permission of the ACM, Inc. To copy otherwise, to republish, to post on servers, or to redistribute to lists requires prior specific permission and/or a fee.

© 20 ACM 0730-0301/20/0100-0001 \$5.00



**Fig. 1:** Comparison of the results predicted by our models against some video of a human iris. (left) One frame of an animation simulating the changes in pupil diameter and iridal pattern deformation. (center) One frame from a video of a human iris. (right) Graph comparing the measured pupil diameters from each individual frame of a nine-second-long video sequence (green line) against the predicted behavior by our model (red line). The gray bars indicate the periods in which the light was kept on and off. The complete video sequence and corresponding animation are shown in the accompanying video.

1920; Calcagnini et al. 2000]. Pupillary light reflex (PLR) is responsible for the constriction of the pupil area in highly lit environments and for its dilation in dimmed ones. PLR is an integral part of our daily experience and, except for drug-induced action, is the single most noticeable of such involuntary movements of the pupil.

The human iris is a muscular tissue containing several easily identifiable structures. Together, they define patterns that are deformed as a result of changes in the pupil diameter. Although pupil light reflex and iridal deformations could be animated using standard computer graphics techniques, such as parametric representations controlled by velocity curves, we believe that the use of physiologically-based models guided by physically meaningful parameters can make the process more predictable and automatic, which, in turn, may result in more realistic and reproducible animations of these movements.

In this paper, we present a physiologically-based model for realistic animation of PLR. Our model combines and extends some theoretical results from the field of Mathematical Biology [Longtin and Milton 1989] with experimental data collected by several researchers relating pupil diameter to the intensity of environmental light [Moon and Spencer 1944]. The resulting model produces high-fidelity appearance effects and can be used to produce real-time predictive animations of the pupil and iris under variable lighting conditions (Section 5.4). We model the iridal pattern deformation process by acquiring a set of high-resolution photographs of real irises at different levels of pupillary dilation and by tracking their features across the set of images. By analyzing the tracked positions, we obtained a simple analytical expression for the iridal deformation pattern as a function of the pupil diameter (Section 6). To the best of our knowledge, ours are the first physiologically-based model for simulating pupil light reflex presented in the graphics literature (the first model ever to simulate individual variability in terms of PLR sensitivity - Section 5.3), as well as the first model for iridal pattern deformation. Moreover, they are the first practical models (*i.e.*, providing actual coefficient values) in the literature for simulating the dynamics of pupil and iris under variable lighting conditions. We demonstrate the effectiveness of our approach by comparing the results predicted by our models against photographs and videos captured from real human irises (Fig. 1 and 12). Table I summarizes the main mathematical and physical quantities used in the derivation of the proposed models and considered throughout this work.

## 2. RELATED WORK IN COMPUTER GRAPHICS

A few researchers have addressed the issue of realistic human iris synthesis. Lefohn et al. [2003] blend several textures created by an artist, each containing some eye feature. Other image-based approaches have

Table I. Summary of the the main mathematical and physical quantities considered in the development of the proposed models.

<i>Symbol</i>	<i>Description</i>	<i>PhysicalUnit</i>
$L_b$	luminance	blondels (B)
$L_{fL}$	luminance	foot-Lambert (fL)
$I_l$	illuminance	lumens/mm <sup>2</sup> ( <i>lm/mm</i> <sup>2</sup> )
$R$	light frequency	Hertz (Hz)
$\phi$	retinal light flux	lumens ( <i>lm</i> )
$\bar{\phi}$	retinal light flux threshold	lumens ( <i>lm</i> )
$D$	pupil diameter	millimeters ( <i>mm</i> )
$A$	pupil area	square millimeters ( <i>mm</i> <sup>2</sup> )
$r_I$	individual variability index	$r_I \in [0, 1]$
$t$	current simulation time	milliseconds ( <i>ms</i> )
$\tau$	pupil latency	milliseconds ( <i>ms</i> )
$x$	muscular activity	none
$\rho_i$	ratio describing the relative position of a point in the iridal disk	none
$\beta, \alpha, \gamma, k$	constants of proportionality	none

been proposed by Cui et al. [2004], Wecker et al. [2005] and Makthal and Ross [2005]. Essentially, they decompose a set of iris images using techniques such as principal component analysis, multiresolution and wavelets, and Markov random fields, and recombine the obtained data to generate new images of irises. Zuo and Schmid [2005] created a fiber-based 3D model of the iris. Lam and Baranoski [2006] introduced a predictive light transport model for the human iris, which computes the spectral responses of iridal tissues described by biophysical parameters. François et al. [2007] estimate iris height maps from gray-scale images. All these approaches use stationary pupil sizes.

Sagar et al. [1994] developed an anatomically detailed model of the eye to be used in a surgical simulator. In their model, Gaussian perturbations were used to simulate the waviness of ciliary fibers and the retraction of pupillary fibers during pupil dilation. Alternatively, depending of the level of object manipulation, a texture mapping approach was used to model the iridal appearance. It is worth noting, however, that their goal was to achieve functional realism [Ferwerda 2003] as opposed to physical or photorealism.

### 3. BRIEF OVERVIEW OF THE HUMAN IRIS AND PUPIL

The human iris has a diameter of about 12mm and forms a disc that controls how much light reaches the retina [Trevor-Roper and Curran 1984]. Under high levels of lighting, the iris dilates, flattening itself and decreasing the pupil size. Under low levels of illumination, it constricts, folding itself and increasing the pupil area. The pupil diameter varies from 1.5mm to 8mm on average [Reeves 1920], and, in general, it is not a perfect circle. Also, its center may deviate from the center of the iris by an offset of up to 20% [Trevor-Roper and Curran 1984]. According to Newsome and Loewenfeld [1971], there are no observable differences in the iris regarding light-induced or drug-induced pupil dilation/constriction.

The human iris is divided in two zones by the *collarette*, a delicate zig-zag line also known as the iris frill. The *pupillary* zone is bounded by the pupil, while the *ciliary* zone extends to the outer border of the iris. Each zone is characterized by a muscle. The *sphincter*, located in the pupillary zone, is a concentric muscle that constricts to decrease the pupil size. The *dilator*, found in the ciliary zone, is a radial muscle that constricts to increase the pupil size. These two muscles overlap at the collarette.

The sphincter and dilator muscles are independently connected to the autonomous nervous system (ANS) [Tilmant et al. 2003] and the pupil size results from a balance of the separately incoming stimuli to the two muscles [Bergamin et al. 1998]. The ANS conducts the pupillary light reflex and *hippus* neural actions. Hippus are spontaneously irregular variations in pupil diameter, which can essentially be characterized as random noise in the 0.05 to 0.3 Hz frequency range [Stark 1939; Usui and Stark 1982]. In PLR, when light

reaches the retina, neural signals are sent to the brain, which sends back a signal for closing or opening the pupil. Thus, PLR can be modeled in two phases: perception and, after some time delay, adjustment.

#### 4. MODELS OF PUPIL DYNAMICS

The pupillometry literature describes several models built around experiments designed to measure the values of some parameters as a function of incident light intensity. Link and Stark [1988] performed a study where a light source was placed in front of the subjects' irises and, by varying the intensity and frequency of the light, they measured the pupillary latency (*i.e.*, the time delay between the instant in which the light pulse reaches the retina and the beginning of iridal reaction):

$$\tau(R, L_{fL}) = 253 - 14 \ln(L_{fL}) + 70R - 29 R \ln(L_{fL}) \quad (1)$$

where  $\tau$  is the latency in milliseconds,  $L_{fL}$  is the luminance measured in foot-Lambert (fL), and  $R$  is the light frequency measured in Hz.

Other similar models predict an average pupil size as a function of the light intensity using a few experimental measurements [Moon and Spencer 1944; de Groot and Gebhard 1952; Pokorny and Smith 1997]. Among those, the most popular one is the Moon and Spencer model [1944], which is expressed as

$$D = 4.9 - 3 \tanh [0.4(\log_{10}(L_b) - 0.5)] \quad (2)$$

where the pupil diameter  $D$  varies from 2 to 8 mm, and  $L_b$  is the background luminance level expressed in blondels, varying from  $10^5$  blondels in sunny days to  $10^{-5}$  blondels in dark nights.  $\tanh$  is the hyperbolic tangent.

##### 4.1 Physiologically-Based Models

In Mathematical Biology and related fields, models based on physiological and anatomical observations were derived to express the relationships among the pupillary action variables without relying on quantitative experimental data. For example, Usui and Stark [1982] proposed a parametric model of the iris to describe the static characteristics of pupil response to light stimuli, and to explain its random fluctuations in terms of probability density functions. Recently, Tilmant *et al.* [2003] proposed a model of PLR based on physiological knowledge and guided by experiments. Although they have obtained plausible results, Tilmant *et al.* have recommended the use of another physiologically-based model to monitor more accurately pupillary dynamics, namely the time-dependent model developed by Longtin and Milton [1989].

Longtin and Milton [1989] define the efferent neural signal  $E(t)$  arriving at the iris per unit of time  $t$ , as

$$E(t) = \beta \ln \left[ \frac{\phi(t - \tau)}{\bar{\phi}} \right] \quad (3)$$

where  $\beta$  is a constant of proportionality and  $\phi$  is the retinal light flux measured in lumens and defined by Stark and Sherman [1959] as  $\phi = I_l A$ : illuminance ( $I_l$ , in lumens/mm<sup>2</sup>) times the pupil area ( $A$ , in mm<sup>2</sup>).  $\tau$  is the latency, and  $\bar{\phi}$  is the retinal light level threshold (*i.e.*, the light level below which there is no change in the pupil area). The notation  $\phi(t - \tau)$  indicates that the current effect depends on the retinal light flux at a time  $\tau$  milliseconds in the past. As the efferent neural signal reaches the iris, it induces some muscular activity  $x$  that may cause the pupil to dilate or constrict. According to Partridge and Benton [1981], the relationship between  $E(t)$  and  $x$  can be approximated by

$$E(t) \cong k \left( \frac{dx}{dt} + \alpha x \right) \quad (4)$$

where  $k$  is a proportionality factor and  $\alpha$  is a rate constant that depends on the definition and units of  $x$

used in the model. Longtin and Milton [1989] combine Equations 3 and 4 as

$$\frac{dx}{dt} + \alpha x = \gamma \ln \left[ \frac{\phi(t - \tau)}{\bar{\phi}} \right] \quad (5)$$

They express the pupil area as  $A = f(x)$  and use the inverse  $f^{-1}(A) = g(A) = x$  to remove  $x$  from Equation 5. In their paper, Longtin and Milton use a Hill function [Hill 1938] (Equation 6) as the function  $f$ , since it can approximate the elasto-mechanical properties of the iris during the pupillary activity:

$$A = f(x) = \frac{\Lambda \theta^n}{\theta^n + x^n} + \Lambda' \quad (6)$$

Here,  $\Lambda'$  and  $\Lambda + \Lambda'$  are, respectively, the minimum and the maximum pupil areas, and  $\theta$  is the value of  $x$  corresponding to the average pupil area. The Longtin and Milton's model then becomes:

$$\frac{dg}{dA} \frac{dA}{dt} + \alpha g(A) = \gamma \ln \left[ \frac{\phi(t - \tau)}{\bar{\phi}} \right] \quad (7)$$

where

$$g(A) = x = \sqrt[n]{\frac{\Lambda \theta^n}{A - \Lambda'} - \theta^n} \quad (8)$$

An S-shaped curve similar to the Hill function has been described in the physiologically-based model of Usui and Stark [1982] to approximate the pupil diameter of an average individual under static illumination conditions.

## 5. THE PROPOSED PHYSIOLOGICAL-BASED MODEL

The model of Moon and Spencer (Equation 2) is based on a set of discrete measurements and approximates the response on an average individual under various lighting conditions. The measurements have been made after the pupil size has stabilized for each illumination level and, therefore, their model does not describe the pupil behavior outside the equilibrium state. Moreover, pupil size, latency, constriction and re-dilation velocities tend to vary among individuals exposed to the same lighting stimulus [Moon and Spencer 1944; Winn et al. 1994]. We remark that such variations are not captured by the model of Moon and Spencer.

Longtin and Milton's model (Equation 7) is time dependent and adaptive, with the potential to handle abrupt lighting changes. It is a theoretical model and, unfortunately, Longtin and Milton did not provide the values for the various parameters in their model (*i.e.*,  $\gamma$ ,  $\alpha$ ,  $\theta$ ,  $n$ ,  $\bar{\phi}$ ), as these, in principle, depend on the abstract notion of iridal muscular activity  $x$ , as well as on the use of the Hill function. The use of incorrect parameter values will not produce realistic results and may cause Equation 7 not to converge.

Starting from the Longtin and Milton's and from Moon and Spencer's models, we derive a practical model that predicts the pupil diameter for the non-equilibrium case based on experimental data (Section 5.2). In Section 5.3, we show how we can extend this basic model to take individual variability into account.

### 5.1 Equilibrium Case

Under constant lighting conditions, the pupil area in the Longtin and Milton's model will converge to an equilibrium state, where

$$\frac{dg}{dA} \frac{dA}{dt} = 0$$

Under such circumstance and assuming there is no occurrence of hippus,  $\phi$  becomes time invariant. Also, recall that  $\ln(m/n) = \ln(m) - \ln(n)$  and, therefore, one can rewrite the Longtin and Milton's model

(Equation 7) for the equilibrium case as:

$$\alpha g(A) = \gamma (\ln(\phi) - \ln(\bar{\phi})) \quad (9)$$

In turn, the Moon and Spencer model can be rewritten as

$$\left( \frac{D - 4.9}{3} \right) = -\tanh \left[ 0.4 \left( \frac{\ln(L_b)}{\ln(10)} - 0.5 \left( \frac{\ln(10)}{\ln(10)} \right) \right) \right]$$

and since the hyperbolic tangent is an odd function, we can rewrite the above equation as

$$-2.3026 \operatorname{atanh} \left( \frac{D - 4.9}{3} \right) = 0.4(\ln(L_b) - 1.1513) \quad (10)$$

where  $\operatorname{atanh}$  is the arc-hyperbolic tangent. Comparing Equations 9 and 10, in order for the Longtin and Milton's model to fit the response of Moon and Spencer's average subject under the equilibrium conditions, one has

$$-2.3026 \operatorname{atanh} \left( \frac{D - 4.9}{3} \right) \approx \alpha g(A) \quad (11)$$

$$0.4(\ln(L_b) - 1.1513) \approx \gamma(\ln(\phi) - \ln(\bar{\phi})) \quad (12)$$

From Equation 12 we can estimate the value of the parameter  $\gamma$ . One should note that  $L_b$  is expressed in blondels while  $\phi$  is given in lumens. Although, in general one cannot convert between two photometric quantities, this can be done under some well-defined situations [Ohta and Robertson 2005]. Since Moon and Spencer's data were collected with the subject seated before a large white screen of uniform intensity which covers most of their field of view, we assume that the light reaching a person's pupil has been reflected by a perfect (Lambertian) diffuse surface. Recall that an ideal (lossless) diffuse reflector returns all of the incident flux so that its reflectance  $\rho = 1$  and its BRDF  $f = 1/\pi$  [Nicodemus et al. 1977]. For such a reflector, 1 blondel =  $10^{-6}$  lumens/mm<sup>2</sup> [Ohta and Robertson 2005].

Since the light flux  $\phi$  depends on the area of the pupil, in order to estimate  $\gamma$ , we first evaluate the left-hand side of Equation 12 for the entire range of illumination covered by the Moon and Spencer's model:  $L_b \in [10^{-5}, 10^5]$  blondels. For each value of  $L_b$ , we then use Equation 2 to estimate  $D$ , from which the pupil area  $A = \pi(D/2)^2$ , and then  $\phi$ , are computed. The retinal light level threshold  $\bar{\phi} = 4.8118 \times 10^{-10}$  lumens was obtained using the pupil diameter  $D_t = 7.8272$  mm, predicted by Equation 2 for  $L_b = 10^{-5}$  blondels (*i.e.*,  $\bar{\phi} = \pi(7.8272/2)^2 \text{ mm}^2 \times 10^{-5} 10^{-6} \text{ lumens/mm}^2$ ). Using the tabulated data for the left-hand side of Equation 12 and the conversion scheme just described, we get the following fitting:

$$0.4(\ln(L_b) - 1.1513) \approx 0.45 (\ln(\phi) - \ln(\bar{\phi})) - 5.2 \quad (13)$$

whose quality of the approximation is illustrated in Fig. 2 (left). The vertical axis of the graph (scaled muscular activity) represents  $\alpha g(A)$ , where  $g(A) = x$  is the muscular activity. The extra constant  $-5.2$  translates the function on right-hand side of Equation 12 vertically, improving the fitting. Given Equation 13, we can replace  $g(A)$  with  $M(D)$  (Equation 11), with  $\alpha = -2.3026$ , where  $M(D)$  is given by

$$M(D) = \operatorname{atanh} \left( \frac{D - 4.9}{3} \right) \quad (14)$$

Thus, the equilibrium situation can be expressed by Equation 15. As expected, it approximates the Moon and Spencer's function (Equation 2) for the pupil diameter of the average subject quite well. The absolute value of the difference between Equations 2 and 15 is under 2% over the entire range of  $[10^{-5}, 10^5]$  blondels

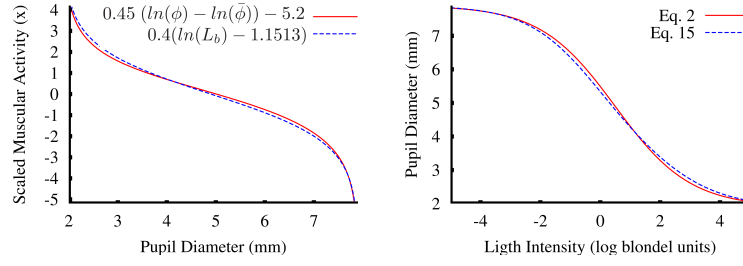


**Fig. 2:** High-quality fittings: (left) Both sides of Equation 13. (right) Equations 2 and 15, whose difference in absolute values is under 2% over the entire range  $[10^{-5}, 10^5]$  blondels.

(Fig. 2 right).

$$2.3026 M(D) = 5.2 - 0.45 \ln \left[ \frac{\phi}{\bar{\phi}} \right] \quad (15)$$

## 5.2 The Dynamic Case

Equation 15 cannot be used to describe the evolution of the pupil diameter in time as a function of instantaneous variations of the light intensity arriving at the pupil. Nevertheless, the obtained constants are still valid for the dynamic case, since the equilibrium is just a special case of the more general pupil behavior, for which the constants should also hold.

In general, one cannot take an equation obtained for the equilibrium and generalize it to the dynamic case. In our model, however, this is possible because of the following constraints:

- $g(A)$  and  $M(D)$  have no explicit time dependence;
- The range of values assumed by  $A$  (or  $D$ ) is the same for both the equilibrium and the non-equilibrium cases;
- There is a one-to-one mapping between  $A$  and  $D$ .

By introducing time in Equation 15, we obtain a delay differential equation that corresponds to our solution for the dynamic case:

$$\frac{dM}{dD} \frac{dD}{dt} + 2.3026 \operatorname{atanh} \left( \frac{D - 4.9}{3} \right) = 5.2 - 0.45 \ln \left[ \frac{\phi(t - \tau)}{\bar{\phi}} \right] \quad (16)$$

where  $D$  and  $\phi$  are expressed in mm and lumens, respectively. For latency  $\tau$ , we use Equation 1 noting that 1 blondel = 0.0929 fL. Pupil constriction velocity is approximately  $3\times$  faster than (re)dilation velocity [Ellis 1981; Bergamin et al. 1998]. We take this difference into account by using different time steps for constriction ( $dt_c$ ) and dilation ( $dt_d$ ) in our numerical solver simulation:

$$dt_c = \frac{T_c - T_p}{S} \quad dt_d = \frac{T_c - T_p}{3S} \quad (17)$$

where  $T_c$  and  $T_p$  are respectively the current and previous simulation times (times since the simulation started) measured in milliseconds,  $S$  is a constant that affects the constriction/dilation velocity and varies among individuals. The higher the  $S$  value, the smaller the time step used in the simulation and, consequently, the smaller the pupil constriction/dilation velocity.

Fig. 3 shows pupil diameter values corresponding to Moon and Spencer's average subject simulated using Equation 16 considering some abrupt changes in the environment luminance. For this example, our results



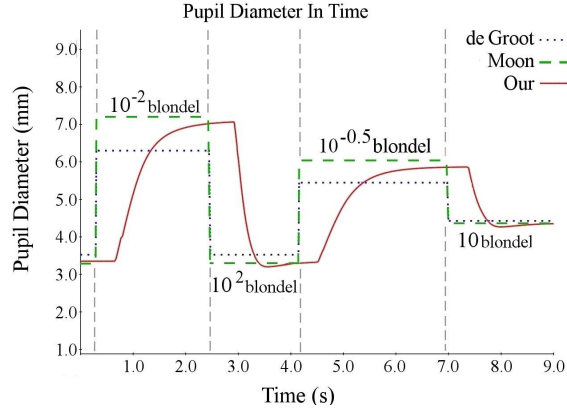


**Fig. 3:** Simulated results produced by our PLR model (Equation 16) for the average subject of Moon and Spencer under non-equilibrium conditions (solid line). For this simulation, the lighting assumed the following values:  $10^{-2}$ ,  $10^2$ ,  $10^{-0.5}$ , and 10 blondels, respectively (delimited by the vertical lines). These results are compared to the static models of Moon and Spencer [1944] (dashed line), and of De Groot and Gebhard [1952] (dotted line). Note the latency predicted by our model.

are compared to results provided by the static models of Moon and Spencer (Equation 2) and of De Groot and Gebhard [1952]

### 5.3 Modeling Individual Differences

While Equation 16 simulates dynamic pupil behavior, it only does so for the average individual represented by the Moon and Spencer model. There are, however, substantial differences in the way pupils from different individuals react to a given light stimulus. Such variations include differences in diameter [Crawford ; Moon and Spencer 1944; de Groot and Gebhard 1952; Ellis 1981; Winn et al. 1994], latency, and constriction and re-dilation velocities [Ellis 1981; Bergamin et al. 1998]. In order to simulate individual differences, we cannot just arbitrarily change the parameter values of our model, as Equation 16 may not converge.

Fig. 4 shows the original data used by Moon and Spencer [1944]. The curve  $C_m$  (shown in black) was obtained by converting the values of  $L_b$  in the range of  $[10^{-5}, 10^5]$  blondels to lumens (see Section 5.1) and then using Equation 15 to compute the corresponding pupil diameter values used for plotting. The top and bottom curves,  $C_t$  and  $C_b$ , respectively, define an envelope containing all pupil diameter values used by Moon and Spencer.  $C_b$  was obtained by fitting a 5 degree polynomial to 11 of the smallest pupil diameter values along the entire luminance range. Likewise,  $C_t$  was obtained by fitting a 5 degree polynomial to 11 of the largest pupil diameter values. We treat  $C_b$ ,  $C_m$  and  $C_t$  as isocurves  $C(p)$  for some parameter  $p \in [0, 1]$ , so that  $C(0) = C_b$ , and  $C(1) = C_t$ . We then model individual differences by associating to each individual  $I$  an index  $r_I \in [0, 1]$  that corresponds to an isocurve  $C(r_I)$ . This index can be randomly generated or, alternatively, it can be recovered from experimental data as described in Section 5.4. To avoid convergence problems and still achieve the results corresponding to isocurve  $C(r_I)$ , we rewrite  $C_t$  and  $C_b$ , respectively, as new functions  $C_{tD}$  and  $C_{bD}$  of the pupil diameter:

$$C_{tD}(D) = -0.013D^5 + 0.322D^4 - 3.096D^3 + 13.655D^2 - 25.347D + 18.179 \quad (18)$$

$$C_{bD}(D) = -5.442D^5 + 1.387D^4 - 1.343D^3 + 6.219D^2 - 1.317D + 1.219 \quad (19)$$

In order to obtain  $C_{tD}$ , we evaluate the functions  $C_m$  and  $C_t$  for  $L_b$  in the range  $[10^{-5}, 10^5]$  blondels, creating ordered pairs of diameter values  $(D_m, D_t) = (C_m(L_b), C_t(L_b))$ . Given enough of these pairs, we fit a curve



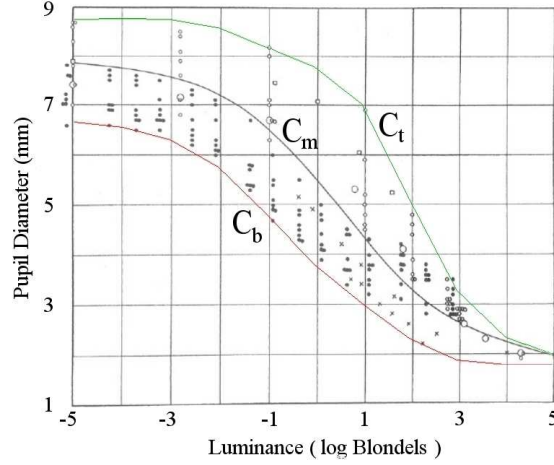


**Fig. 4:** Original data used by Moon and Spencer [1944]. The curve  $C_m$  corresponds to Equation 15. The pair of curves  $C_b$  and  $C_t$  define an envelope containing all data.

expressing  $D_t$  as a function of  $D_m$  (or  $D$  for short). The resulting curve is  $C_{tD}$  (Equation 18). The case of  $C_{bD}$  is similar. The final pupil diameter at any time is then obtained solving Equation 16 for  $D$  and then evaluating

$$D_{final} = C_{bD}(D) + (C_{tD}(D) - C_{bD}(D))r_I \quad (20)$$

We have adopted this solution due to its simplicity and generality: we can easily replace the curves  $C_{bD}(D)$  and  $C_{tD}(D)$  with new ones, covering new data as they become available, or representing other models (*e.g.*, De Groot and Gebhard [1952]). Since the relative distances of  $C_m$  to  $C_b$  and  $C_t$  vary for different values of  $D$ , no value of  $r_I$  will exactly recover  $C_m$ . This is not a problem, however, as  $C_m$  correspond to the average subject. Other parameterizations are possible, including ones that interpolate  $C_m$  for a given value of  $r_I$ .

Although our model properly simulates the elastic behavior of the iris muscular activity during changes in lighting conditions, it does not model hippus (*i.e.*, Equation 16 will converge to some pupil diameter value if the lighting conditions remain constant). As random fluctuations whose causes are still unknown [Usui and Stark 1982; Ukai et al. 1997], it is currently not possible to define a physiologically-based model for hippus. We visually approximate the hippus effect by adding small random variations to the light intensity (between  $-10^{0.3}$  and  $10^{0.3}$  blondels), to induce small variations in the pupil diameter (of the order of 0.2 mm [Hachol et al. 2007]), in the frequency range of 0.05Hz to 0.3Hz. This significantly improves the realism of the resulting simulations and animations. According to Usui and Stark [1982], the standard deviation of the noise corresponds to approximately 10% of the pupil diameter.

#### 5.4 The PLR Model Validation

In order to validate our PLR model under non-equilibrium conditions and to show that it is capable of representing individual variability, we performed some qualitative comparisons between actual pupil behavior and the results of simulations produced by our model. For this, we captured videos of normal subjects presenting significantly different light sensitivities (*i.e.*, different PLR responses), while a light was turned *on* and *off* several times. Since pupil constriction is bigger when both eyes are stimulated [Thomson 1947], the subjects kept both eyes opened. To avoid fatigue and habituation of the iris [Lowenstein and Loewenfeld 1964], in each experiment we recorded less than one minute of video per subject.

We computed the pupil diameters of the subjects at each frame of the video sequences. Lighting measure-

ments made during video capture were used as input to our PLR model for simulating pupil behavior. The pupil diameters resulting from these simulations were then compared to the pupil diameters computed at individual video frames. Note that the simulated results are not expected to quantitatively match the observed ones, but rather be in qualitative agreement with observed behavior.

The videos were captured using a Cannon ELURA2 miniDV camcorder (NTSC,  $720 \times 576$  pixels) with progressive scan connected to a PC through a firewire connection. We kept the room's light dimmed so that the subjects' pupils could dilate naturally to some extent, but not too dark that we could not see the pupils in the individual video frames. Because of these constraints, we used two subjects (both males) with light eyes (a 24-year-old with green eyes, and a 26-year-old with blue eyes). For each frame, the pupil diameters were estimated from the set of dark pixels (pupil area  $P_{area}$ ) inside a specified rectangle containing solely the subject's pupil and part of the iris (Fig. 5). Given  $P_{area}$ , the pupil diameter was obtained (assuming the pupil is a circle) as  $d = 2(\sqrt{P_{area}/\pi})$  pixels. The conversion from pixels to millimeters was performed considering a typical iris diameter of 12 mm. According to our experience, computing the pupil diameter as described produces more accurate results than computing it as the number of pixels in the largest straight segment in the set of dark pixels (the pupil).

Since the video frames were captured at approximately 30 Hz, in practice no variation is expected between the pupil diameters in neighbor frames under constant illumination, even in the presence of hippus. Thus, we estimated the average error in the computed pupil diameters to be approximately 0.1 mm by computing the average difference between estimated pupil diameters for neighbor frames. Based on the video sequences, we set  $S = 600$  (Equation 17) for the two subjects in all experiments, as this value made their simulated constriction velocities approximate the ones in the video sequences. We empirically set the frequency of the two light sources used in our experiments to  $R = 0.4$  Hz, a value that made the latency estimated by Equation 1 approximate the latency observed in the video frames.

To evaluate the quality of our simulations, we performed experiments with both subjects using two different kinds of light sources to induce pupil constriction: a small flashlight and a 100 Watt incandescent white light bulb. For light measurements, we used an LD-200 Instrutemp digital lux meter (precision  $\pm 3\%$ , frequency 2Hz).

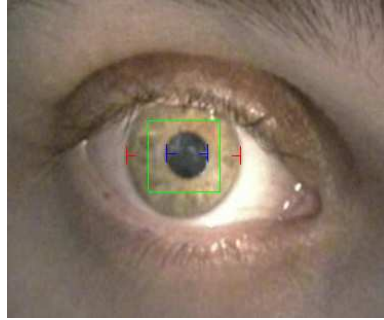


**Fig. 5:** Estimating pupil diameter from a rectangular region containing only the pupil and some iris pixels. The pupil diameter is estimated from the area occupied by the dark pixels, assuming a circular pupil and an iris with diameter of 12 mm.

**5.4.1 The Flashlight Experiments.** In these experiments, we used a light source to induce significant changes in the subjects' pupil diameters without introducing considerable changes in the environment lighting conditions. For this purpose, we used a small flashlight powered by a single AAA battery (1.5 Volt) kept at about 20 cm from the subject's right eye and pointed at it. Given the small area illuminated by

the flashlight as well as it reduced power, the readings from the lux meter were very sensitive to even small changes in the relative position and orientation of the flashlight with respect to lux meter sensor. Thus, we decided to run two simulations using the recorded data: (i) considering the light intensity estimated using Equation 2, and (ii) considering the readings from the lux meter. These two experiments are explained next.

**The first flashlight experiment:** In this experiment, we used the Moon and Spencer equation (Equation 2) to solve for the light intensities during the *on* and *off* states of the flashlight, based on the measured pupil diameters (from the video). Since the Moon and Spencer function (curve  $C_m$  in Fig. 4) represents the pupil behavior of an average individual, we estimated the *on* (*off*) light intensity as the average of the computed *on* (*off*) intensities for both subjects. Using this procedure, we obtained estimates of  $10^{1.1}$  blondels when the flashlight was on, and  $10^{-0.5}$  blondels when the flashlight was off. Given the average luminance value for the *on* (*off*) state and the corresponding pupil diameter for a given subject, we used Equation 20 to estimate the  $r_{I_{on}}$  ( $r_{I_{off}}$ ) index for that subject. The subject's final  $r_I$  index was computed as the average between his  $r_{I_{on}}$  and  $r_{I_{off}}$  indices. Using this procedure, we obtained  $r_I = 0.4$  for the green-eye subject and  $r_I = 0.03$  for the blue-eye subject.

Fig. 6 shows the actual pupil diameter measurements performed on a frame-by-frame basis along 9-second-long sequences captured for each subject. The green '+' marks on top represent the measurements for the green-eye subject, while the blue 'x' marks show the measurements of the blue-eye subject. This example illustrates the inter-subject variability in terms of light sensitivity and shows the ability of our model to appropriately represent such individual differences. The vertical dotted lines delimit the intervals in which the flashlight was kept on and off for each subject. The solid and dashed lines represent the simulated results produced by our model for the green-eye and blue-eye subjects, respectively, and closely agree with the actual measured values. These curves were produced automatically from Equations 16 and 20, on top of which we added small random variations (hippus effect) as described in the previous section. The accompanying video shows side-by-side comparisons of our simulated results and videos captured for the two subjects.

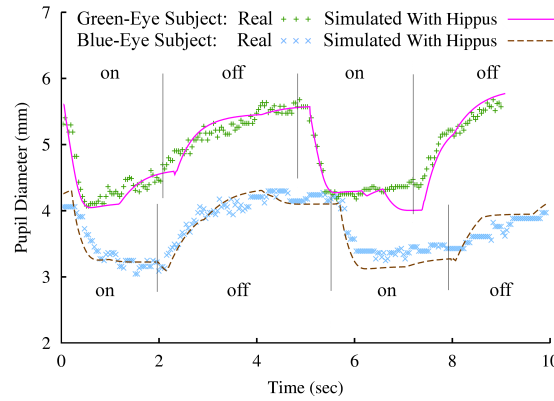


**Fig. 6:** Comparison between our simulated results and measurements from real video sequences using the flashlight as stimulus. The green '+' and the blue 'x' marks represent, respectively, the pupil diameter measurements for the green-eye and for the blue-eye subjects, obtained for all frames along a 9-second-long video sequence. The solid and dashed lines are the pupil diameters predicted by our physiologically-based model for the green-eye and for the blue-eye subjects, respectively, after random noise (hippus effect) has been added. The vertical dotted lines delimit the intervals in which the flashlight was kept on and off for each subject. The predicted values closely agree with the actual measured values.

**The second flashlight experiment:** In this experiment, we used the readings provided by the lux meter

for the *on* and *off* states of the flashlight. These illuminance values were 350 lux<sup>1</sup> and 90 lux, respectively. One should recall that in such a setup, small changes in the position and orientation of the subject's head produce changes in the illuminance at the pupil. Therefore, these values are only approximations to the actual illuminance reaching each subject's lit eye. Given the illuminance values and the subjects' corresponding pupil diameters estimated from the video frames, we obtained the actual pupil's luminous flux (in lumens) at the two flashlight states, for each individual. These values were then converted to blondels according to the assumption described in Section 5.1. We then used Equations 16 and 20 to estimate their corresponding  $r_I$  indices (by averaging  $r_{I_{on}}$  and  $r_{I_{off}}$ ), obtaining  $r_I = 0.54$  for the blue-eye subject and  $r_I = 0.92$  for the green-eye subject. Fig. 7 compares the actual pupil measurements (same as in Fig. 6) with the results simulated by our model using the lux meter readings as input. The differences between the simulated curves shown in Fig. 6 and 7 are primarily due to the added random noise (hippus).

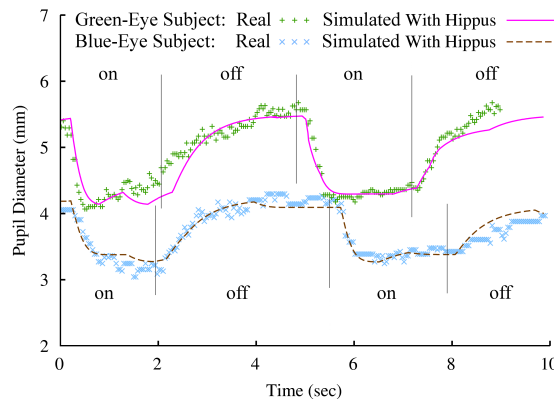


**Fig. 7:** Similar to the graphs shown in Fig. 6 but using the illuminance readings provided by the lux meter as input to our model. The simulated results, including hippus, for the green-eye and blue-eye subjects are shown as solid and dashed lines, respectively.

**5.4.2 The 100 Watt Lightbulb Experiment.** For this experiment we used a more stable light source to induce pupil constriction: a spot with a 100 Watt incandescent white lightbulb, kept at about one meter in front and one meter to the right of the subject's head. This setup allowed the subjects to remain comfortable with their eyes opened while the light was on.

We measured the environment light intensity during the *on* and *off* states by positioning the digital lux meter at approximately the same position and orientation of the subject's right eye. During the blue-eye subject experiment, we found the illuminance to be equal to 140 lux when the light was off and 315 lux when it was on. During the green-eye subject experiment, the readings were 91 and 540 lux, respectively. These differences resulted from a darker environment and a slight approximation of the green-eye subject to the light source. Again, we used the illuminance values and the subjects' corresponding pupil diameters (measured from the video) as input to Equations 16 and 20 to estimate their corresponding  $r_I$  indices (by averaging  $r_{I_{on}}$  and  $r_{I_{off}}$ ). We obtained  $r_I = 0.9$  for the blue-eye subject and  $r_I = 1.0$  for the green-eye subject.

Fig. 8 (top) shows the actual pupil diameter measurements performed on a frame-by-frame basis along 56 and 50-second-long sequences captured for the blue-eye and for the green-eye subjects, respectively. The

<sup>1</sup>1 lux = 1 lumen/m<sup>2</sup>

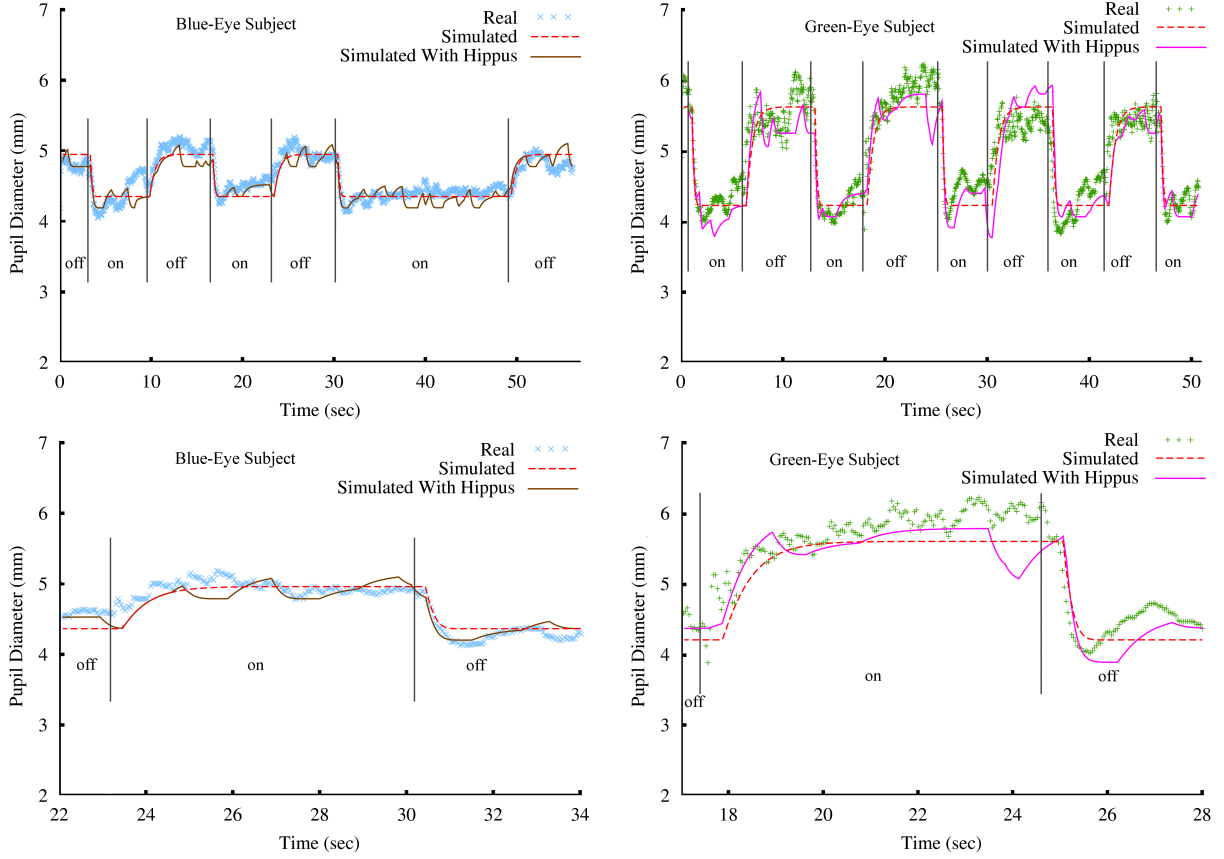


**Fig. 8:** Comparison between our simulated results and measurements from real video sequences using light emitted by a lightbulb as stimulus. The 'x' and '+' marks represent the pupil diameter measurements for the blue-eye (left) and for the green-eye (right) subjects, respectively. Top row: values obtained for all frames along a 56- and 50-second-long video sequence, respectively. The solid and dashed lines are the pupil diameters predicted by our physiologically-based model with and without hippus, respectively. The vertical lines delimit the intervals in which the incandescent light bulb was kept on and off for each subject. The predicted values match the actual measurements well. The bottom row shows zoomed versions of the graphs shown on the top.

vertical lines delimit the intervals in which the light was kept *on* and *off* for each subject. The solid and dashed lines represent the simulated results produced automatically by our model (Equations 16 and 20) with and without hippus, respectively, and closely agree with the actual measurements. Fig. 8 (bottom) shows zoomed versions of portions of the graphs shown on top, exhibiting *off-on-off* transitions.

One should note that the simulated results produced by our PLR model closely approximate the actual behaviors of the subjects' pupils in all three experiments, illustrating the effectiveness of our model. The differences in the  $r_I$  indices for a given subject among the experiments can be explained as:

- In the two flashlight experiments, the pupil diameters used for the *on* and *off* states were the same, but the illuminance values provided by Equation 2 and by the lux meter were different. The different indices simply reflect the different light sensitivities presented to our model as input;
- When comparing the 100 Watt lightbulb and the flashlight experiments, both the lighting and the pupil

sizes varied for the *on* and *off* states of the light sources. For instance, for the green-eye subject, the pupil diameters were approximately 4.3 mm and 5.7 mm for the *on* and *off* states of the flashlight, respectively (Fig. 7). This resulted in a  $r_I$  index of 0.92. In the case of the 100 Watt lightbulb experiment, these values were approximately 4.3 mm and 6.0 mm, respectively (Fig. 8), with  $r_I = 1.0$ . These two indices are relatively close and reflect the difference in the maximum pupil diameters between the two experiments. The difference in the  $r_I$  indices for the blue-eye subject were considerably bigger, from 0.54 to 0.9. Again, this can be explained by comparing the measured pupil diameters in the two experiments. These values went from approximately 3.2 mm and 4.2 mm in the *on* and *off* states of the flashlight (Fig. 7) to 4.4 mm and 5.2 mm in the *on* and *off* states of the 100 Watt lightbulb (Fig. 8).

An important point to note is that by using an average of the estimated  $r_I$  indices for the *on* and *off* states of the light source, our model is capable of realistically simulating the pupil behavior of individuals with considerable differences in PLR responses under different and variable lighting conditions.

## 6. MODELING THE IRIS DEFORMATION

Although the iris is a well-known structure [Freddo 1996], there is no general agreement about a model of its behavior. Rohen [Rohen 1951] seems to have been the first researcher to study the form of the collagen structure of the iris. He suggested that the collagen fibers are arranged in a series of parallel arcs, connecting the iris root with the pupil border, clockwise and counterclockwise in an angle of 90 degrees oriented by the center of the pupil. These fibers would be interwoven with other iris components, such as blood vessels. Based on the Rohen's fiber arrangement, Wyatt [2000] proposed a 2D non-linear model for iris deformation. Such a model has been validated on canine, porcine and monkey iris, but so far not on human irises [Wyatt 2007].

We derived our model for iridal pattern deformation by analyzing sets of photographs taken from five volunteers under controlled conditions. In our experiments, an eye doctor dilated their pupils with some mydriatic drug and we photographed their irises at several stages during the pupil dilatation process using a Canon PowerShot SD 400 camera with macro lens. The images were taken at the resolution of  $2,048 \times 1,536$  pixels, and were then cropped to square images containing only the iris and pupil. After cropping, the smallest image was  $800 \times 800$  pixels and the larger ones were rescaled to fit the same dimensions. Thus, let  $S_i = \{I_{i1}, I_{i2}, \dots, I_{in}\}$  be the set of  $n$  images from a given volunteer  $V_i$  taken along the pupil dilation process. For each image  $I_{ij}$ , we positioned a circle on the outer border of the iris and another one at the border of the pupil (the two circles delimit the iridal disk). We also defined the center of the pupil as the center of the inner circle. We then manually marked a series of iridal feature points and tracked them along the set of images of each volunteer. Fig. 9 (left) shows an image with the tracked features indicated by a set of colored dots. The complete set of images used for tracking the iridal features of this volunteer is shown in Fig. 10.

Fig. 9 (right) shows how the positions of the individually tracked iridal feature points changed along the dilation process. The trajectories of the points both on the pupillary and ciliary zones move on approximately radial paths. Although some imprecision in the exact location of the points might have resulted from the manual specification, most of the deviation from the radial paths result from the existence of blood vessels under the iris, and from crypts, and folds (the iris folds its tissue as a result of pupil dilation) that prevent iris points from always moving along radial lines. Such structures vary considerably among individuals but, according to our experience, their influence on the paths of the feature points usually have small magnitude (Fig. 9 right). Therefore, as a first approximation, we can assume that the iris points move along straight lines in the radial directions. It is worth noting that Wyatt's 2D model [Wyatt 2000] does not take the influence of these structures into account either.

In order to find how fast the feature points moved, we computed the following measures during the dilation process: (i) the distance from the tracked feature point to the pupil center; (ii) the distance from the tracked



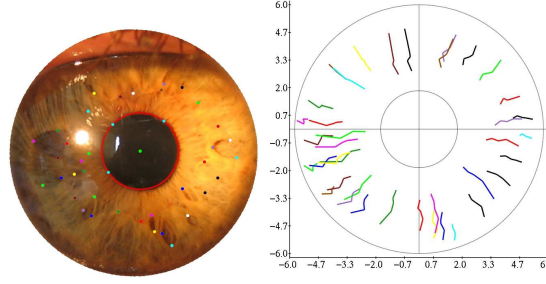


**Fig. 9:** Left: Photograph of a volunteer's iris taken during the dilation process. The colored dots indicate tracked feature points and the center of the pupil. Right: Evolution of the positions of the individually tracked points during the dilation process. Each feature point is identified by a different color.

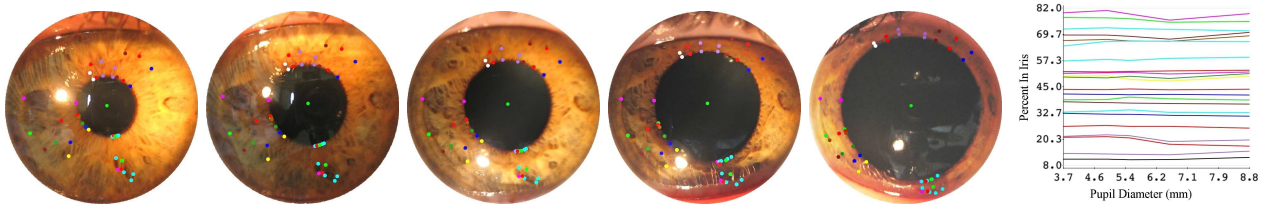


**Fig. 10:** Set of images used to track the iridal features of a volunteer along the dilation process. Color dots indicate corresponding points in the different images. From left to right, the pupil diameter values are: 3.70, 4.94, 5.53, 6.57, and 8.81 mm, respectively. The apparent changes in iris color are due to the changes in the position of the light source used to illuminate the subject's eye (the camera's flash was turned off). The graph on the right shows evolution of the ratio defined by Equation 21 for all tracked feature points along the dilation process. The graph shows 22 out of 50 tracked points for one subject (due to space constraints). This pattern of an approximately constant ratio was observed for all subjects and all tracked points.

feature point to the pupil border; and (iii) the ratio between the distance from the tracked point to the pupil border and the local width of the iridal disk (*i.e.*, the distance from the pupil border to the external iris border measured along the radial segment passing through the feature point). One should recall that the pupil is not necessarily circular and that its center does not necessarily coincide with the center of the iris. While measurements (i) and (ii) presented a pretty much linear behavior, the ratio represented by (iii) was approximately constant for all feature points (Fig. 10 right). The same behavior was observed in the irises of all five volunteers. Like the variations in the trajectories of the points shown in Fig. 9 (right), the deviations from horizontal lines in Fig. 10 (right) are caused by the subjects' iris structures, specially the iridal folds. Again, as a first approximation, the following ratio can be assumed constant for any iridal point  $p_i$ , for all values of pupil diameters:

$$\rho_i = \frac{\|p_i - c_i\|}{\|E_i - c_i\|} \quad (21)$$

where  $p_i$  be a point on the iris disk,  $c_i$  and  $E_i$  are the points on the pupil border and on the iris outer circle, respectively, such that they are collinear to the radial segment passing through  $p_i$ .  $\|\cdot\|$  is the  $L^2$  (Euclidean) norm. The invariance expressed by Equation 21 summarizes the observations illustrated in Fig. 10 (right) and is the basis of our image-based model for iridal pattern deformation.





**Fig. 11:** Examples of iris rendered using our PLR and iridal pattern deformation models. Images simulated for light intensities of  $10^5$  blondels (left) and 1 blondel (right), for the Moon and Spencer’s average subject. Note that the pupil is offset from the center of the iris disk. No light reflection on the corneal surface has been simulated to avoid masking iris details.

### 6.1 Animating the Deformed Iridal Patterns

As an approximation to the behaviors depicted in Figs. 9 (right) and 10 (right), we use texture mapping to animate the iris deformation process. Note that this is a natural and efficient way of implementing the behavior modeled by Equation 21: as the pupil dilates/constricts, the iris ring is compressed/stretched, but the parameterization (in the  $[0, 1] \times [0, 1]$  domain) of the points inside the ring remains the same. Thus, for animation purposes, we model the iris as a planar triangle-strip mesh on the disk defined by the two circles and use a photograph of an iris with a small pupil diameter as a texture. Texture coordinates map the border of the pupil to the inner circle of the mesh, and outer border of the iris to the mesh’s outer circle. Currently, we tessellate the mesh creating a pair of triangles at every five degrees. The animation proceeds by computing the new pupil diameter  $D$  as a function of the incident lighting using Equation 20. We then reposition each vertex  $v_i$ , located on the inner circle of the mesh, at a distance  $D/2$  along the radial line connecting the center of the pupil to  $v_i$ , while keeping their original texture coordinates unchanged. One should recall that the center of the pupil does not necessarily match the center of the iris, and thus, it is important to keep the coordinates of the center of the pupil. Fig. 11 shows the renderings of an iris created using our models for different lighting conditions. Note that the patterns deform in a natural way. No light reflection on a corneal surface has been simulated to avoid masking iris details. Fig. 12 compares the results produced by our models with actual photographs. Note that the deformed patterns closely approximate the ones in the photographs.

## 7. DISCUSSION

We have implemented the proposed models and used them to render synthetic images of the human iris and pupil. The resulting animations are very convincing and run in real time. We have compared the images produced by our models with photographs and videos of real human irises. The results produced by our models are in qualitative agreement with observed behavior in humans.

In order to demonstrate the potential use of the proposed models in computer graphics, we built an application that renders a human head model in an environment illuminated by HDR cube maps (see accompanying video). The head model was obtained from [Turbo Squid 2007] and its original irises were replaced by our textured triangle-strip model. The HDR images were obtained from Paul Debevec’s web site [Debevec 2007] and are used to approximate the environment’s radiance. As the head looks at different parts of the environment, its pupil diameters adapt to the irradiance in the solid angle defined by its field of view, producing pleasing animation effects.

Accommodation and age affect the pupil diameter [Winn et al. 1994] and iris color influences some PLR parameters, such as maximum pupil diameter, latency, and constriction velocity [Bergamin et al. 1998]. These aspects are currently not taken into account by our model because the lack of reliable data over a large range of lighting conditions. For instance, Winn [1994] discusses the effect of age on the size of the

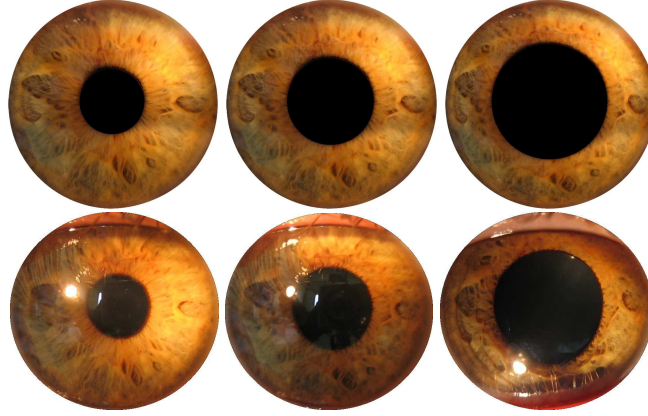


**Fig. 12:** Comparison of our simulated results with a set of photographs. Top: renderings produced using our pupil light reflex and iridal pattern deformation models for environments with 35,638.7, 3,102.52, and 71.85 lumens/mm<sup>2</sup>, respectively. No light reflection on the corneal surface has been simulated to avoid masking iris details. Bottom: photographs of a human iris. Note the realistic deformation of the iridal patterns.

pupil. His study, however, only considered luminance values from  $10^1$  to  $10^4$  blondels, which corresponds to only about 30% of the luminance range used by our model. Currently, we model variations in pupil diameters for the same light stimulus using Equation 20, which can be used to simulate the age-related miosis effect reported by Winn. Also, since our model covers the entire range of valid pupil diameter values, it safely covers the pupillary sizes resulting from influence of attentional and other cognitive factors. Extending our model to handle other phenomena based on biophysical parameters is an interesting direction for future work.

No relief data representing the iris folds are used in the current version of the model, as it is done in the technique presented by [François et al. 2007]. Also, no corneal refraction is used. Thus, at grazing angles, in addition to the distortion resulting from pupil dilation/constriction, one would perceive the projective distortion due to texture mapping. Relief information could be added to our model in a straightforward way, allowing some interesting shading effects such as projected shadows and self-occlusions [Policarpo et al. 2005; Oliveira and Policarpo 2005].

We use a linear model for iridal pattern deformation even though the actual deformation is non-linear. However, according to Wyatt [Wyatt 2000], such non-linearity contributes approximately only 1% of the diameter of a typical iris (12.0 mm). Most of the non-linear behavior seen in Fig. 9 (right) and Fig. 10 (right) are due to the interference of folds and blood vessels, which vary among individuals. To the best of our knowledge, no model in the literature takes those factors into account.

Many other factors affect pupil size [Tryon 1975], including particular states of mind, such as interest and curiosity [Hess and Polt 1964], spectral sensitivity [Werner 2003], respiratory and heart rate [Calcagnini et al. 2000], and spatial patterns in the visual field [Li et al. 2006]. Taking all these aspects into account seems to be impractical due to their inherent complexity and limited supporting data. We should emphasize that PLR causes the single most noticeable involuntary movements of the pupil. As the graphs depicted in Figs. 7 and 8 and the accompanying video show, our PLR model alone can produce predictable animations of the pupil dynamics.

## 8. CONCLUSION

We have presented new models for realistic renderings of the human iris and pupil. Our physiologically-based model of the pupil light reflex combines and extends theoretical results from the Mathematical Biology field [Longtin and Milton 1989] with experimental data collected by several researchers [Moon and Spencer 1944]. The resulting model is expressed in terms of a non-linear delay-differential equation that describes the changes in the pupil diameter as function of the environment lighting. Our model is also original in the sense that it can simulate individual differences with respect to light sensitivity. As all parameters of our models were derived from experimental data, they correctly simulate the actual behavior of the human iris and pupil. They also produce high-fidelity appearance effects, which can be used to create real-time predictive animations of the pupil and iris under variable lighting conditions. We have validated our models through comparisons of our simulated results against videos and photographs captured from human irises. The quality of these simulations qualitatively matched the actual behaviors of human pupils and irises.

To the best of our knowledge, ours is the first physiologically-based model for simulating pupil light reflex presented in the graphics literature. It is also the first practical model (*i.e.*, providing actual coefficient values) in the literature for simulating the dynamics of pupil and iris under variable lighting conditions, and the first integrated model in all literature to consider individual variability in pupil diameter using general equations for latency and velocity. Our image-based model for iridal pattern deformation is also the first model of its kind in the graphics literature. Our results should find applicability in several areas requiring high-fidelity facial animations, as well as on feature film animations, where the request for increasing levels of realism never ends.

We believe that this work can also contribute to investigations outside the scope of computer graphics. More specifically, the simulation tools presented in this paper can be used to complement wet experiments and accelerate the hypothesis evaluation cycle in ophthalmological and physiological research. It is worth mentioning that computer simulations are being successfully and routinely used by biologists and medical researchers to study the predictive behavior of living systems under various conditions, including some not yet experimentally tested [Ventura et al. 2006].

## ACKNOWLEDGMENTS

We are grateful to the following people for resources, discussions and suggestions: Prof. Jacobo Melamed Cattán (Ophthalmology-UFRGS), Prof. Roberto da Silva (UFRGS), Prof. Luis A. V. Carvalho (Optics-USP/SC), Prof. Anatolio Laschuk (UFRGS), Leandro Fernandes, Marcos Slomp, Leandro Lichtenfelz, Renato Silveira, Eduardo Gastal, and Denison Tavares. We also thank the volunteers who allowed us to collect pictures and videos of their irises: Alex Gimenes, Boris Starov, Christian Pagot, Claudio Menezes, Giovane Kuhn, João Paulo Gois, Leonardo Schmitz, Rodrigo Mendes, and Tiago Etienne. Manuel M. Oliveira acknowledges a CNPq-Brazil fellowship (305613/2007-3). Gladimir V. G. Baranoski acknowledges a NSERC-Canada grant (238337). Microsoft Brazil provided additional support.

## REFERENCES

- BERGAMIN, O., SCHOETZAU, A., SUGIMOTO, K., AND ZULAUF, M. 1998. The influence of iris color on the pupillary light reflex. *Graefes Arch Clin Exp Ophthalmol* 236(8), 567–570.
- CALCAGNINI, G., CENSI, F., LINO, S., AND CERUTTI, S. 2000. Spontaneous fluctuations of human pupil reflect central autonomic rhythms. *Methods Inf Med.* 39(2), 142–145.
- CRAWFORD, B. H. The integration of the glare effects from a number of glare sources. *Proc. Phys. Soc.* 48(1), 35–37.
- CUI, J., WANG, Y., HUANG, J., TAN, T., AND SUN, Z. 2004. An iris image synthesis method based on PCA and super-resolution. In *Proc. of 17th ICPR*. IEEE Comp. Soc., Washington, USA, 471–474.
- DE GROOT, S. G. AND GEBHARD, J. W. 1952. Pupil size as determined by adapting luminance. *J. Opt. Soc. Am.* 42, 492–495.
- DEBEVEC, P. 2007. Paul Debevec’s home page. <http://www.debevec.org/>.

- ELLIS, C. J. 1981. The pupillary light reflex in normal subjects. *British Journal of Ophthalmology* 65(11), 754–759.
- FERWERDA, J. 2003. Three varieties of realism in computer graphics. In *Proceedings of SPIE Human Vision and Electronic Imaging*. The International Society for Optical Engineering, 290–297.
- FRANÇOIS, G., GAUTRON, P., BRETON, G., AND BOUATOUCH, K. 2007. Anatomically accurate modeling and rendering of the human eye. In *SIGGRAPH '07: Sketches*. ACM, New York, USA, 59.
- FREDDO, T. 1996. Ultrastructure of the iris. *Microscopy Research and Technique* 33, 369–389.
- HACHOL, A., SZCZEPANOWSKA-NOWAK, W., KASPRZAK, H., ZAWOJSKA, I., DUDZINSKI, A., KINASZ, R., AND WYGLEDOWSKA-PROMIENSKA, D. 2007. Measurement of pupil reactivity using fast pupillometry. *Physiol. Meas.* 28, 61–72.
- HESS, E. H. AND POLT, J. M. 1964. Pupil size in relation to mental activity during simple problem-solving. *Science* 143, 1190–1192.
- HILL, A. V. 1938. The heat of shortening and the dynamic constants of muscle. *Proc R Soc London B Biol Sci* 126, 136–195.
- LAM, M. W. Y. AND BARANOSKI, G. V. G. 2006. A predictive light transport model for the human iris. *Computer Graphics Forum* 25 (3), 359–368.
- LEE, S., BADLER, J., AND BADLER, N. 2002. Eyes alive. *ACM Transactions on Graphics* 21, 3, 637–644.
- LEFOHN, A., BUDGE, B., SHIRLEY, P., CARUSO, R., AND REINHARD, E. 2003. An ocularist's approach to human iris synthesis. *IEEE Comput. Graph. Appl.* 23, 6, 70–75.
- LI, Z., LIANG, P., AND SUN, F. 2006. Properties of pupillary responses to dynamic random-dot stereograms. *Exp Brain Res* 168, 436–440.
- LINK, N. AND STARK, L. 1988. Latency of the pupillary response. *IEEE Trans. Bio. Eng.* 35(3), 214–218.
- LONGTIN, A. AND MILTON, J. G. 1989. Modelling autonomous oscillations in the human pupil light reflex using non-linear delay-differential equations. *Bulletin of Math. Bio.* 51 (5), 605–624.
- LOWENSTEIN, O. AND LOEWENFELD, I. E. 1964. The sleep-waking cycle and pupillary activity. *NYAS Annals* 117, 142–156.
- MAKTHAL, S. AND ROSS, A. 2005. Synthesis of iris images using markov random fields. In *Proc. of EUSIPCO*. Antalya, Turkey.
- MOON, P. AND SPENCER, D. 1944. On the stiles-crawford effect. *J. Opt. Soc. Am.* 34, 319–329.
- NEWSOME, D. AND LOEWENFELD, I. 1971. Iris mechanics. ii. influence of pupil size on dynamics of pupillary movements. *Am J Ophthalmol.* 71, 1 Part 2 (Jan), 353–373.
- NICODEMUS, F. E., RICHMOND, J. C., HSIA, J. J., GINSBERG, I. W., AND LIMPERIS, T. 1977. Geometrical considerations and nomenclature for reflectance. Tech. rep., National Bureau of Stds, Washington, DC. Inst. for Basic Stds. Oct.
- OHTA, N. AND ROBERTSON, A. 2005. *Colorimetry: fundamentals and applications*. John Wiley & Sons, Chichester, England.
- OLIVEIRA, M. M. AND POLICARPO, F. 2005. An efficient representation for surface details. Tech. Rep. RP-351, UFRGS, Porto Alegre, Brazil.
- PARTRIDGE, L. D. AND BENTON, L. A. 1981. *Handbook of Physiology, Motor Control*. Vol. 2. American Physiological Society, Washington, Chapter Muscle: The Motor, 43–106.
- POKORNY, J. AND SMITH, V. C. 1997. The verriest lecture. How much light reaches the retina? In *C.R. Cavonius (ed), Colour Vision Deficiencies XIII. Doc. Ophth. Proc. Series* 59, 491–511.
- POLICARPO, F., OLIVEIRA, M. M., AND COMBA, J. L. D. 2005. Real-time relief mapping on arbitrary polygonal surfaces. In *I3D '05: Proceedings of the 2005 symposium on Interactive 3D graphics and games*. ACM, New York, NY, USA, 155–162.
- REEVES, P. 1920. The response of the average pupil to various intensities of light. *J. Opt. Soc. Am.* 4(2), 35–43.
- ROHEN. 1951. Der bau der regenbogenhaut beim menschen und einigen sugern. *Gegenbaur Morphology Journal* 91, 140–181.
- SAGAR, M., BULLIVANT, D., MALLINSON, G., HUNTER, P., AND HUNTER, I. 1994. A virtual environment and model of the eye for surgical simulation. *SIGGRAPH, Annual Conference Series*, 205–213.
- STARK, L. W. 1939. Stability, oscillations, and noise in the human pupil servomechanism. *Proc. of the IRE* 47(11), 1925–1939.
- STARK, L. W. AND SHERMAN, P. M. 1959. A servoanalytic study of consensual pupil reflex to light. *J. Neurophysiol.* 20, 17–26.
- THOMSON, L. C. 1947. Binocular summation within the nervous pathways of the plr. *J. Physiology* 106, 59–65.
- TILMANT, C., CHARAVEL, M., PONROUCH, M., GINDRE, G., SARRY, L., AND BOIRE, J.-Y. 2003. Monitoring and modeling of pupillary dynamics. *Proc. of 25th IEEE EMBS* 1, 678–681.
- TREVOR-ROPER, P. D. AND CURRAN, P. V. 1984. *The Eye and Its Disorders*. Vol. 3. Blackwell Scientific Publications, Oxford, Boston, Chapter The Eyeball, 3–75.
- TRYON, W. W. 1975. Pupillometry: A survey of sources of variation. *Psychophysiology* 12, 1, 90–93.
- TURBO SQUID. 2007. 3d max male face head. <http://www.turbosquid.com/FullPreview/Index.cfm/ID/357993>.
- UKAI, K., TSUCHIYA, K., AND ISHIKAWA, S. 1997. Induced pupillary hippus following near vision: increased occurrence in visual display unit workers. *Ergonomics* 40, 11 (Nov.), 1201–1211.

- USUI, S. AND STARK, L. 1982. A model for nonlinear stochastic behavior of the pupil. *BioCyber* 45, 1 (Aug), 13–21.
- VENTURA, B., LEMERLE, C., MICHALODIMITRAKIS, K., AND SERRANO, L. 2006. From *in vivo* to *in silico* biology and back. *Nature* 443, 527–533.
- WATT, A. AND WATT, M. 1992. *Advanced Animation and Rendering Techniques*. Addison-Wesley, New York.
- WECKER, L., SAMAVATI, F., AND GAVRILOVA, M. 2005. Iris synthesis: a reverse subdivision application. *GRAPHITE '05*, 121–125.
- WERNER, A. 2003. Spectral sensitivity of the pupillary system. *Clin. Exp. Optom.* 86(4), 235–238.
- WINN, B., WHITAKER, D., ELLIOTT, D. B., AND PHILLIPS, N. J. 1994. Factors affecting light-adapted pupil size in normal human subjects. *IOVS* 35(3).
- WYATT, H. J. 2000. A minimum-wear-and-tear meshwork for the iris. *Vision Research* 40, 2167–2176.
- WYATT, H. J. 2007. Private communication, on oct. 20.
- ZUO, J. AND SCHMID, N. A. 2005. A model based, anatomy based method for synthesizing iris images. In Proc. of ICB 2006, Hong Kong, China. *ICBA*, 428–435.

Received Month Year; revised Month Year; accepted Month Year